Earth's Future

RESEARCH ARTICLE
10.1029/2022EF002671

Future Co-Occurrences of Hot Days and Ozone-Polluted Days Over China Under Scenarios of Shared Socioeconomic Pathways Predicted Through a Machine-Learning Approach

Cheng Gong[1], Ye Wang[2], Hong Liao[2], Pinya Wang[2], Jianbing Jin[2], and Zhiwei Han[3]

[1]State Key Laboratory of Atmospheric Boundary Layer Physics and Atmospheric Chemistry LAPC, Institute of Atmospheric Physics, Chinese Academy of Sciences, Beijing, China, [2]Jiangsu Key Laboratory of Atmospheric Environment Monitoring and Pollution Control, Jiangsu Collaborative Innovation Center of Atmospheric Environment and Equipment Technology, School of Environmental Science and Engineering, Nanjing University of Information Science and Technology, Nanjing, China, [3]Key Laboratory of Regional Climate-Environment for Temperate East Asia, Institute of Atmospheric Physics, Chinese Academy of Sciences, Beijing, China

Key Points:

- A machine-learning approach was developed to quantify the climatological risk level of ozone (O_3) pollution during hot days over China
- Co-occurrence of O_3-polluted days and hot days reduced from 3.7 days in 2030s to 3.0 days in 2050s over China under the Shared Socioeconomic Pathway (SSP) 1-2.6 scenario
- The SSP 5-8.5 scenario led to higher co-occurrences of O_3-polluted days and hot days in 2050s, especially in North China and northwest China

Supporting Information:

Supporting Information may be found in the online version of this article.

Correspondence to:

H. Liao,
hongliao@nuist.edu.cn

Citation:

Gong, C., Wang, Y., Liao, H., Wang, P., Jin, J., & Han, Z. (2022). Future co-occurrences of hot days and ozone-polluted days over China under scenarios of Shared Socioeconomic Pathways predicted through a machine-learning approach. *Earth's Future*, *10*, e2022EF002671. https://doi.org/10.1029/2022EF002671

Received 13 JAN 2022
Accepted 20 MAY 2022

Author Contributions:

Conceptualization: Cheng Gong, Hong Liao
Data curation: Ye Wang
Formal analysis: Cheng Gong
Funding acquisition: Hong Liao, Zhiwei Han
Investigation: Cheng Gong
Methodology: Cheng Gong, Ye Wang, Jianbing Jin
Project Administration: Zhiwei Han

Abstract The warming climate increases the probability of hot days, which leads to a penalty effect of increasing ozone (O_3)-polluted days in polluted regions. Here, we established a random forest algorithm to predict future probabilities of O_3 exceedance (P) during hot days and further examined the future co-occurrences of O_3-polluted days and hot days under two different scenarios of Shared Socioeconomic Pathways (SSPs) 1-2.6 and 5-8.5 for 2030–2050s. Ground-level observations, simulated O_3-temperature sensitivities in the GEOS-Chem model, multimodel seasonal-mean O_3 concentrations and daily maximum temperature from the sixth Coupled Model Intercomparison Project (CMIP6), leaf area index from reanalyzed data, and local geographical information were comprehensively utilized. Evaluations showed that the algorithm captured the spatial patterns of present-day P values well with a correlation coefficient of 0.92 over China. Results showed that the strong reductions in anthropogenic emissions under SSP 1-2.6 significantly reduced the risks of O_3 exceedance during hot days nationwide from 3.7 days in the 2030s to 3.0 days in the 2050s. However, the SSP 5-8.5 scenario witnessed more frequent co-occurrences of O_3-polluted days and hot days over the 2030–2050s with nationally averaged values from 4.5 to 6.4 days. Our results highlight the co-benefits of reducing anthropogenic emissions to alleviate the composite risks of extreme weather events and air-polluted days in the future.

Plain Language Summary Temperature is generally considered as the most important meteorological factor that influences ground-level ozone (O_3) concentrations. A warmer climate is highly likely to lead to frequent occurrence of hot days, which could further increase ozone-polluted days in regions with high anthropogenic emissions. The co-occurrences of O_3-polluted days and hot days lead to composite risks to human health, but how such co-occurrences will change in the future is rarely examined. Here, we established a novel machine-learning approach by using a random forest algorithm to quantify the probability of O_3 exceedance (P) during hot days and then predicted the future co-occurrence of O_3-polluted days and hot days under two different future emission scenarios (Shared Socioeconomic Pathways [SSP]1-2.6 and SSP5-8.5). Multisource data, including ground-level observations, reanalyzed data, GEOS-Chem simulations, and multimodel outputs from Coupled Model Intercomparison Project, were comprehensively utilized. We found that the random forest algorithm was capable to derive a reasonable pattern of P values over China. Composite risks of O_3 exceedance during hot days are projected to be reduced significantly in the future under the SSP 1-2.6 scenario, whereas to keep increasing until the 2050s under the SSP 5-8.5 scenario.

1. Introduction

Tropospheric ozone (O_3) is an important secondary air pollutant detrimental to both human health (Fleming et al., 2018; Kuerban et al., 2020; Lelieveld et al., 2015) and terrestrial ecosystems (Gong, Yue, et al., 2021; Lombardozzi et al., 2015; Yue et al., 2017). It is produced by photochemical reactions of nitrogen dioxide ($NO_x = NO + NO_2$) and volatile organic compounds (VOCs) (Kleinman et al., 2002; Sillman, 1999) and removed by redox chemical reactions and deposition processes (Clifton et al., 2020; Jacob & Winner, 2009). Currently, eastern China is confronted with the most severe O_3 pollution in the world (Lu et al., 2018). Since 2013, the

Resources: Pinya Wang
Supervision: Hong Liao
Visualization: Cheng Gong
Writing – original draft: Cheng Gong
Writing – review & editing: Hong Liao, Pinya Wang

summertime mean O_3 concentrations as well as the frequencies of O_3-polluted days (defined as average maximum daily 8-hr (MDA8) O_3 concentrations larger than 80 ppbv in this study based on Gong et al. (2020)) have been increasing over eastern China (Gong et al., 2020; Li et al., 2019; Lu et al., 2020). Understanding how global changes, especially changes in anthropogenic emissions and climate, influence the frequency of O_3-polluted days is essential to execute proper control strategies.

Temperature was identified to have the strongest impacts on O_3 concentrations among all meteorological factors in most regions with high anthropogenic emissions (Dawson et al., 2007; Shi et al., 2020; Steiner et al., 2006). High temperature increases O_3 concentrations by processes that include enhancing biogenic emissions of volatile organic carbon (BVOCs) (Gong, Liao, et al., 2021; Ma et al., 2019) and accelerating chemical reactions (Wang et al., 2017). Specifically, O_3-polluted days tend to occur on hot days (defined as daily maximum temperature (Tmax) exceeding 35°C in this study) (Pu et al., 2017; J. L. Schnell & Prather, 2017). For example, Solberg et al. (2008) examined the strong heat waves in June–August 2003 over Europe and showed that extremely high temperatures led to maximum O_3 concentrations exceeding 230 μg m^{-3} at most observed sites. Analitis et al. (2014) analyzed data in nine European cities from 1990 to 2004 and showed that high O_3 concentrations during hot days increased daily deaths by 54% among people aged 75–84 years compared to the deaths induced by hot days alone, suggesting composite health risks associated with co-occurrence of hot days and O_3-polluted days.

The Sixth Assessment Report by the Intergovernmental Panel on Climate Change (IPCC) (https://www.ipcc.ch/report/ar6/wg1/) showed that global temperature will continue to increase until 2050s even with the strictest emission control measures under scenarios of Shared Socioeconomic Pathways (SSPs) 1-1.9. A warmer climate has a high likelihood of bringing a "penalty effect" on O_3 in polluted regions (Bloomer et al., 2009; Fu & Tian, 2019). For instance, Colette et al. (2015) composited projections of 25 models from 11 published studies and found that future climate scenarios have penalty effects on summertime surface O_3 of at most 5 ppbv over Europe from 2071 to 2100. Schnell et al. (2016) assembled projected O_3 from four global models with fixed anthropogenic ozone precursors. They showed that warming under the RCP8.5 scenario increased the summer-mean O_3 of about 4–10 ppbv in eastern U.S, 1–5 ppbv in southern Europe, and 3–6 ppbv in northeastern Asia in the 2100s compared to the 2000s. To better indicate the intensity of the "climate penalty on O_3," Wu et al. (2008) proposed a "climate penalty factor," which is represented by the sensitivity of O_3 to Tmax (dO_3/dT) and has been widely used (Bloomer et al., 2009; Fu et al., 2015; Gu et al., 2020; Rasmussen et al., 2013; Zhao et al., 2013). In addition, a warmer climate increases the probability of hot days (Ding et al., 2010; Perkins-Kirkpatrick & Lewis, 2020), which further increases the probability of the occurrences of severe O_3-polluted days. However, to our knowledge, the future co-occurrence of O_3-polluted days and hot days under different emission scenarios has rarely been examined.

Simulations of future hot days and future O_3-polluted days usually rely on Earth System Models (ESMs) with fully coupled NO_x-O_3-hydrocarbon-aerosol chemical mechanisms (Meehl et al., 2018). However, current ESMs generally use a simplified O_3 chemistry scheme (Lamarque et al., 2013) to reduce the computational burden, which would cause uncertainties in the simulated future O_3. Furthermore, a quite limited number of ESMs (to our knowledge, only one model, namely UKESM1-0-LL) in the recent Sixth Coupled Model Intercomparison Project (CMIP6) simultaneously provide both future daily temperature and hourly O_3 concentrations under different projected emission scenarios (e.g., SSP1-2.6 and SSP5-8.5) (https://esgf-node.llnl.gov/projects/cmip6/). Instead, the multimodel-predicted monthly mean Tmax and O_3 concentrations, which potentially represent the risks of co-occurrence of hot days and O_3-polluted days, are assessable. As a result, we aim to fully utilize the multimodel results to avoid the one-model dependence problem and better predict future co-occurrence of hot days and O_3-polluted days.

In this study, we established a machine-learning approach by using a random forest algorithm to quantify the climatological risk level of O_3 pollution during hot days and then further predicted the future co-occurrence of O_3-polluted days and hot days under two different projected emission scenarios (SSP1-2.6 and SSP5-8.5). Section 2 describes the framework of this study based on the random forest algorithm and further introduces the data, including site-level observed data, reanalyzed meteorological data, simulations from the 3D global chemical transport model (GEOS-Chem), and multimodel results from CMIP6. In the results section, the current risk level of O_3 pollution during hot days over China since 2013 is shown. Then, we establish and evaluate the

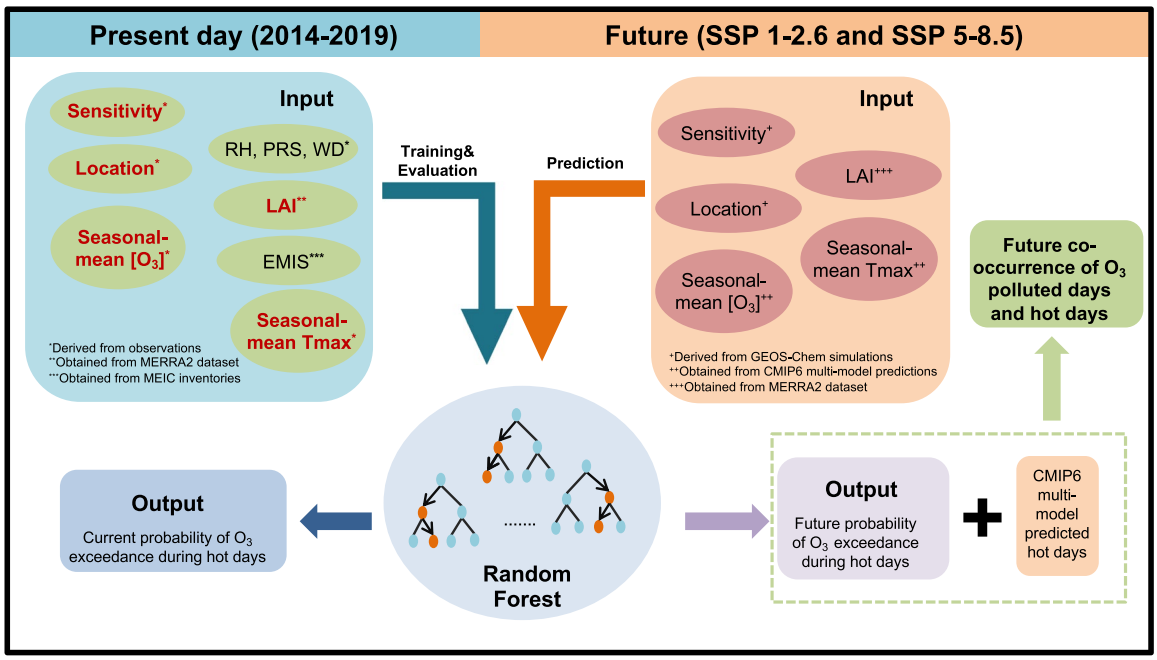

Figure 1. Summary of the procedures to predict future co-occurrences of O_3-polluted days and hot days. The red parameters in the present day input indicate the selected parameters used in the random forest algorithm (see Table 1 and Section 3.2).

machine-learning approach and predict the future co-occurrence of O_3-polluted days and hot days. Finally, we draw conclusions and discuss the uncertainties and implications of this study.

2. Data and Methods

2.1. Framework of Predicting the Future Co-Occurrences of O_3-Polluted Days and Hot Days

In this study, we introduced the probability of O_3 exceedance *(P)* during hot days to reflect the climatological risk level of co-occurrence of O_3-polluted days and hot days. Present-day *P* can be represented by the following equation:

$$P = \frac{OD_H}{HD} \times 100\% \quad (1)$$

where *HD* is the number of hot days, and OD_H is the number of O_3-polluted days that occurred on all hot days at one specific site or grid. The *P* value is calculated only when the *HD* is larger than 3 days over May–October in 1 year.

We aimed to predict future *P* values through a framework of the random forest algorithm with the help of multi-source data (Figure 1). To begin with, the random forest algorithm was trained and evaluated to predict the present-day *P* values in China over May–October in 2014–2019 based on observed data. Then, we applied the established random forest algorithm to predict future *P* values in the 2030, 2040s, and 2050s under SSP 1-2.6 and SSP 5–8.5 scenarios with the help of GEOS-Chem simulations (providing O_3-Tmax sensitivities) and CMIP6 multimodel predictions (providing daily mean Tmax and monthly mean O_3 concentrations). Finally, we derived future co-occurrences of O_3-polluted days and hot days by multiplying future *P* values from the random forest algorithm and projected hot days in CMIP6 ensembles.

In particular, we applied the O_3-Tmax sensitivities (*S*) following the definition in Wu et al. (2008) to better achieve the prediction of *P*:

$$[MDA8\,O_3] = S \times Tmax + b \quad (2)$$

where [*MDA8* O_3] and Tmax are the daily series of MDA8 O_3 concentrations and Tmax over May–October at a specific site or grid, respectively; and *S* and *b* are the annual sensitivity of MDA8 O_3 concentrations to temperature and the residuals, respectively, both of which are obtained by least square fitting. The present-day *S* values were derived from site-level observations (see details in Section 2.3), while the future *S* values under different scenarios were from GEOS-Chem simulations (see details in Section 2.4). Since *S* represents the enhancement of O_3 concentrations with an increase in temperature of 1°C, high *S* values implied a high probability of the occurrence of O_3-polluted days during hot days.

2.2. Random Forest Algorithm

As a traditional machine-learning approach with the capability to solve complex regressions and classification problems, the random forest algorithm has been widely used in the field of atmospheric chemistry in recent years (Araki et al., 2018; Chen et al., 2018; Kaminska, 2019; Wang et al., 2019; Wei et al., 2019; Zhan et al., 2018). A random forest consists of a large number of individual decision trees, which are grown on dependent bootstrap samples from training data sets. Each decision tree divides bootstrap samples into branches through decision nodes until a leaf node is attained. Leaf nodes represent predicted estimates of one simple decision tree, and the mean prediction of the individual trees is determined as the regression output of the random forest algorithm (Breiman, 2001).

In this study, the function *RandomForestRegressor* of the python package *scikit-learn* was applied (Pedregosa et al., 2011). To predict the probability of O_3 exceedance (*P* in Equation 1) during hot days, we composited a series of related predictors, including O_3-Tmax sensitivity (*S* in Equation 2), latitude, longitude, seasonal-mean meteorological factors, O_3 concentrations, reanalyzed leaf area index (LAI), and anthropogenic NO_x and VOCs emissions, to test the random forest algorithm. The number of decision trees was 200. To be consistent with the future grid-level input data in the random forest model, we used the 1° × 1° (rather than site-level) predictors for 2014–2017 from the observations and reanalysis as the training data and evaluated the random forest by using data in 2018–2019 with two indicators: correlation coefficient (R) and root mean square error (RMSE).

2.3. Observed O_3 and Meteorological Data

The ground-level hourly observed O_3 concentrations were obtained from the monitoring network established by the Ministry of Ecology and Environment (MEE) of China (http://www.cnemc.cn). We then derived the MDA8 O_3 concentrations for all 1,582 sites (Figure S1 in Supporting Information S1) over May–October in 2014–2019 and interpolated site-level data to 1° × 1° for further application in the random forest algorithm.

Four observed daily meteorological factors, namely the Tmax, daily mean relative humidity (RH), pressure (PRS), and wind speed (WS), were obtained from ground-level weather monitoring stations maintained by the China Meteorological Administration (http://data.cma.cn/). The meteorological data observed at more than 600 sites (Figure S1 in Supporting Information S1) were interpolated into O_3 observed sites by averaging the meteorological values at the nearest five sites within a 2-degree square domain.

2.4. GEOS-Chem-Simulated O_3-Tmax Sensitivities

The GEOS-Chem model is a state-of-art 3D global chemistry transport model with good capabilities in simulating the spatiotemporal variations in gas phase pollutants and aerosols (Dang & Liao, 2019; Li et al., 2019; Porter & Heald, 2019). It is driven by MERRA2 reanalyzed data from the Goddard Earth Observing System (GEOS) of the NASA Global Modeling and Assimilation Office (GMAO) and employs a fully coupled NO_x-O_x-hydrocarbon-aerosol chemistry mechanism. The vertical resolution of GEOS-Chem is 47 layers from the surface to 0.1 hPa. Photolysis rates are computed by the Fast-JX scheme (Bey et al., 2001; Park et al., 2003; Pye et al., 2009). Stratospheric O_3 is simulated by linearized ozone parameterization (LINOZ) following McLinden et al. (2000). A nonlocal scheme in planetary boundary layers is applied to describe the vertical mixing process (Lin & McElroy, 2010). The Model of Emissions of Gases and Aerosols from Nature (MEGAN v2.1) is utilized to dynamically calculate biogenic VOCs emissions (Guenther et al., 2012).

In this study, we first performed simulations over May–October during 2014–2019 in the Asian nested domain (11°S–55°N, 60°–150°E) with horizontal resolutions of latitude 0.5° × longitude 0.625°. The lateral boundary

layers of all chemical tracers were provided by global simulations at a resolution of 2° latitude × 2.5° longitude. Anthropogenic emissions over China were obtained from the annually updated Multi-resolution Emission Inventory (MEIC, http://www.meicmodel.org) (Zheng et al., 2018). It should be noted that the present-day simulated results were not used in the random forest algorithm but were designed to evaluate model performance in simulating O_3-Tmax sensitivities and to further revise future simulated *S* values.

Since many previous studies have shown that the decadal variations in *S* values in polluted regions were determined by the changes in anthropogenic emissions (Bloomer et al., 2009; He et al., 2013; Jing et al., 2017; Rasmussen et al., 2013; Wu et al., 2008), we further derived future *S* values from GEOS-Chem simulation with fixed meteorology in 2015 and future anthropogenic emissions (years 2030, 2040, and 2050) under SSP 1-2.6 and SSP 5–8.5 scenarios. Furthermore, those simulations were only performed at a global resolution of 2° latitude × 2.5° longitude to better integrate data from climate-system models in CMIP6 with coarse horizontal resolutions.

2.5. CMIP6 Multimodel Outputs

To perform a reasonable prediction of future changes in temperature and surface O_3, we applied the daily Tmax data from 18 climate models in CMIP6 and the monthly mean surface O_3 data from 11 chemistry climate coupling models (Table S1 in Supporting Information S1) (downloaded from https://esgf-node.llnl.gov/projects/cmip6/). Model outputs with the "r1i1p1f1" variant in two scenarios (SSP 1-2.6 and SSP 5-8.5) were selected. The horizontal resolutions of variables from different models were integrated to a resolution of latitude 2° × longitude 2.5° by bilinear interpolation. Seasonal-mean (May–October) values (such as Tmax and O_3 concentrations) as well as the number of hot days were further derived for the present-day (2015), 2030s (averaged over 2028–2032), 2040s (averaged over 2038–2042), and 2050s (averaged over 2048–2052).

2.6. Auxiliary Data

Two sets of data were applied as an auxiliary to establish the random forest algorithm. One data set was the daily grid-level LAI from the MERRA2 reanalyzed data set with horizontal resolutions of latitude 0.5° × longitude 0.625°, considering the significant impacts of vegetation on O_3 as revealed by many previous studies (Gong, Liao, et al., 2021; Lin et al., 2020). The other data set was the monthly mean anthropogenic NO_x and VOCs emissions from MEIC over 2014–2017. We scaled the MEIC emissions in 2018–2019 based on national emission trends reported by the MEE following Li et al. (2021).

3. Results

3.1. Present Day Probability of O_3 Pollution During Hot Days Over China

Figures S2a and S2b in Supporting Information S1 show the seasonal mean MDA8 O_3 concentrations and the number of hot days over May–October during 2014–2019 in China. The seasonal mean MDA8 O_3 concentrations in North China (35°N–41°N and 110°E−120°E) were high and showed rapid increases from a regionally averaged 51.9 ppbv in 2014 to 70 ppbv in 2019. Meanwhile, the number of hot days averaged over all observed sites in North China also showed an increasing trend from 6.8 days in 2014 to 12.4 days in 2019, which was reported as one of the important factors for explaining the increased O_3 concentrations by previous studies (Wei et al., 2021).

Figure S2c in Supporting Information S1 shows that O_3 exceedances became increasingly frequent during hot days over 2014–2019 in North China, where the *P* values sharply increased from 47.2% in 2014% to 88.9% in 2019 on average. Considering the increasing number of hot days, the average co-occurrence of O_3-polluted days and hot days in North China also increased from 3.2 (6.8*47.2%) days in 2014 to 11.0 (12.4*88.9%) days in 2019. The increasing *P* may have been caused by many reasons. For example, increases in seasonal mean O_3 concentrations as well as O_3-Tmax sensitivities (Figure S3 in Supporting Information S1) are likely important factors, and the changes in meteorology and anthropogenic emissions may also be influential. To quantify the complex and nonlinear relationships between *P* values and those potential predictors, the random forest algorithm was established and evaluated to predict the future risks of the co-occurrence of O_3-polluted days and hot days.

Table 1
Eight Experiments of the Random Forest Algorithm Using Different Predictors

Name	Predictors	Score	RMSE (%)
EX1	S	0.48	20.9
EX2	S, lat, lon	0.60	18.5
EX3	S, lat, lon, O_3	0.72	15.5
EX4	S, lat, lon, O_3, Tmax	0.73	15.2
EX5	S, lat, lon, O_3, Tmax, LAI	0.75	15.0
EX6	S, lat, lon, O_3, Tmax, LAI, Mete	0.72	15.7
EX7	S, lat, lon, O_3, Tmax, LAI, Emis	0.74	15.3
EX8	S, lat, lon, O_3, Tmax, LAI, Mete, Emis	0.72	15.2

Note. Detailed descriptions of each predictor are shown in Table S2 in Supporting Information S1. Score (the coefficient of determination) and RMSE were derived between the observed and random-forest-predicted P values on 1° × 1° grids in China averaged over May–October during 2018–2019 following these two formulas: $\text{Score} = 1 - \frac{\sum_i \sum_j \left(P_{rf,i,j} - P_{obs,i,j}\right)^2}{\sum_i \sum_j \left(P_{obs,i,j} - \overline{P_{obs}}\right)^2}$, $\text{RMSE} = \sqrt{\frac{\sum_i \sum_j \left(P_{obs,i,j} - P_{rf,i,j}\right)^2}{n}}$, where $P_{obs,i,j}$ and $P_{rf,i,j}$ indicate the observed and random-forest-predicted P values in the gird with i latitude and j longitude. $\overline{P_{obs}}$ are observed P values averaged over all grids in China. n represents the total number of 1° × 1° grids in China.

3.2. Establishment and Evaluation of the Random Forest Algorithm

We used the 1° × 1° grid-level data over 2014–2017 as the training data and designed eight random forest experiments (EX1-EX8) to select the most effective and essential predictors to predict *P* values. All experiments included the predictor of O_3-Tmax sensitivity *S* because high *S* values implied a high probability of the occurrence of O_3-polluted days during hot days. In EX1, only *S* was considered, and we further added latitude-longitude geographic information, seasonal-mean O_3 concentrations, Tmax, LAI, other meteorological factors (RH, PRS, and WS), and anthropogenic NO_x and VOCs emissions step-by-step for EX2-8. A detailed description of each predictor is shown in Table S2 in Supporting Information S1. Table 1 shows the random-forest score (the coefficient of determination) and RMSE over all grids in China between the observed and random-forest-predicted *P* values during the warm season in 2018–2019. The variables *S*, latitude, longitude, and seasonal-mean O_3 concentrations were the most effective predictors of *P*, and the score reached 0.72 and the RMSE decreased to 15.5% in EX3. Including the seasonal mean Tmax and LAI slightly improved the performance of random forest although the other three meteorological factors as well as the anthropogenic NO_x and VOCs emissions had opposite effects. As a result, the configuration of EX5 was determined as the final random forest algorithm.

Figure 2 shows the spatial patterns of observation-derived and EX5-predicted *P* values averaged over May–October in 2018–2019. The observation-derived *P* values at the 1° × 1° grids (Figure 2a) were generally lower than the site-level observations (Figure S2c in Supporting Information S1) because the interpolation exaggerated the spatial scales and thus enhanced the difficulty of determining the co-occurrences of O_3-polluted days and hot days at the grid level. The random forest algorithm captured the spatial distributions of *P* values ($R = 0.92$) well with a mean bias of −4.4% nationwide. However, the current random forest configuration underestimated the risk of O_3 exceedance during hot days in extremely polluted regions, such as North China, where the predicted *P* value only reached 56.9% on average compared to the observed values of 73.5%.

3.3. Processing of Simulated Input Data for Future Prediction

3.3.1. GEOS-Chem-Simulated *S* Values

Since many previous studies have shown that GEOS-Chem can well simulate the spatial patterns as well as interannual variations in seasonal-mean O_3 concentrations (e.g., Li et al. (2019); Lu et al. (2019); Y. Wang et al. (2011)), we mainly focused on the evaluation of O_3-Tmax sensitivity over 2014–2019. Figure S4a in Supporting Information S1 shows high spatial correlations between site-level observed and GEOS-Chem-simulated *S* values with $R = 0.75$. However, the simulated *S* values were significantly underestimated, especially in severely polluted

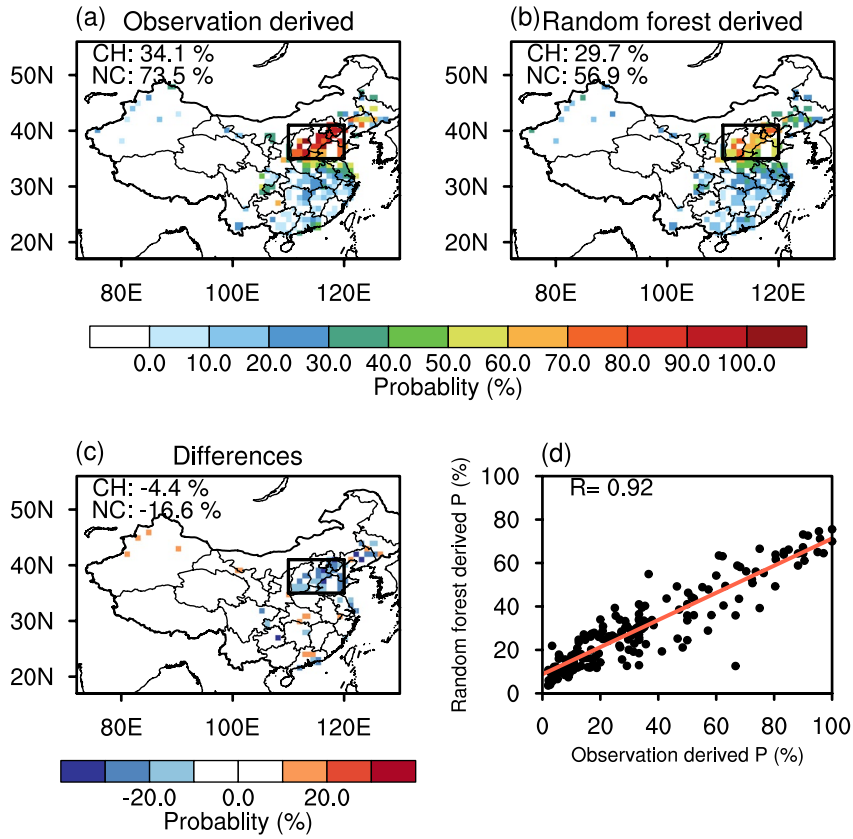

Figure 2. Spatial patterns of (a) observation-derived, (b) EX5-predicted *P* values, and (c) their differences averaged over May–October in 2018–2019. Numbers labeled "CH" and "NC" represent values averaged over China and North China (enclosed by black rectangles), respectively. (d) Linear regressions and spatial correlation coefficients between observations and random forest predictions. Each dot indicates a *P* value at one 1° × 1° grid.

regions such as North China, which were likely to be induced by the underestimates of extremely high O_3 concentrations in GEOS-Chem when hot days occurred (Gong & Liao, 2019; Gong et al., 2020).

To alleviate the underestimates, we further revised the simulated *S* values in the present-day simulations and applied the revision in future GEOS-Chem simulations. To begin with, we found that the underestimates were mainly induced by regions with high *S*. For all grids with the observed *S* larger than 2 ppbv K^{-1}, the mean observed *S* was 2.7 ppbv K^{-1}, while the mean simulated *S* only reached 1.8 ppbv K^{-1}. As a result, we applied a ratio of 1.5 (2.7/1.8) to revise the *S* values for all simulated girds and then kept *S* that is lower than 2 ppbv K^{-1} unchanged as the original simulated values. In this way, the normalized mean bias was significantly reduced from −33.8% to −9.8% nationwide (Figure S4b in Supporting Information S1).

3.3.2. Selection of CMIP6 Models

We selected 5 model outputs of Tmax from 18 CMIP6 models, including AWI-CM, CanESM5, CMCC-ESM2, INM-CM4-8, and MPI-ESM1-HR, by comparing the daily Tmax under the SSP 5–8.5 scenario in 2015 to MERRA2 reanalyzed data over China following the three criteria: (a) correlation coefficients of seasonal mean Tmax between simulations and MERRA2 at all grids over China should exceed 0.5 (Figure S5 in Supporting Information S1); (b) the mean bias of seasonal-mean Tmax over China should be lower than 1°C (Figure S6 in Supporting Information S1); and (c) the mean bias of hot days over China should be lower than 5 days (Figure S7 in Supporting Information S1). The comparison of MERRA2 to CMIP6 model outputs under the SSP 1-2.6 scenario is not shown here because similar patterns with SSP 5-8.5 were induced by the same anthropogenic climate forcings of 2015.

The patterns of seasonal-mean O_3 concentrations from 11 chemistry climate models in 2015 are shown in Figure S8 in Supporting Information S1. Only 5 models showed valid O_3 concentrations over the mainland, and MPI-ESM-2-HR and MPI-ESM-2-LR (also NorESM2-LM and NorEMS2-MM) were not independent of each

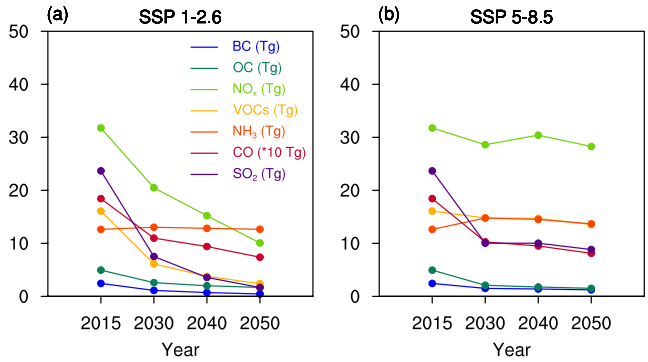

Figure 3. Future changes in annual anthropogenic emissions of different air pollutants, including black carbon, organic carbon, nitrogen oxide, volatile organic compounds, ammonia, carbon monoxide, and sulfur dioxide, under the (a) Shared Socioeconomic Pathway (SSP) 1-2.6 and (b) SSP 5-8.5 scenarios over China in the years of 2015, 2030, 2040, and 2050, respectively.

other. To obtain as much independent data from different models as possible, we averaged the simulated future O_3 concentrations in BCC-CSM2-MR, MPI-ESM1-2-HR, NorESM2-LM, and the simulated O_3 concentrations in GEOS-Chem with future emissions but fixed the meteorology as the future seasonal-mean O_3 fields to predict future *P* values in the random forest algorithm. The GEOS-Chem simulations were also used because the global transport chemistry model generally has more comprehensive chemical mechanisms than most of the climate models (Lamarque et al., 2013). Although the climate conditions were fixed in 2015, the GEOS-Chem model applying future anthropogenic emissions was still able to describe reasonable patterns of seasonal-mean O_3 concentrations (Figure S8 in Supporting Information S1) and further balance the bias in climate models.

3.4. Predicted Future Co-Occurrences of O_3-Polluted Days and Hot Days

To better understand the predicted results from the random forest algorithm, we first compared two different emission scenarios (SSP 1-2.6 and SSP 5-8.5). Since it is well known that SSP 1-2.6 and SSP 5-8.5 represent low and high levels of future greenhouse gas emissions, respectively (Meinshausen et al., 2020); here, we focus on the anthropogenic emissions of air pollutants (such as ammonia (NH_3), NO_x, VOCs, sulfur dioxide (SO_2), and carbon monoxide (CO)). In the SSP 1-2.6 scenario, almost all air pollutants in China show marvelous emission reductions in the future, except for NH_3 (Figure 3a). Especially, the two most important O_3 precursors, NO_x and VOCs, reduced from 31.8 Tg to 16.1 TgC in 2015 to 10.1 Tg and 2.4 TgC in 2050, respectively. Such drastic changes are mainly contributed by the reductions in eastern China (Figures S9 and S10 in Supporting Information S1), implying where the future O_3 pollution would be significantly alleviated under the SSP 1–2.6 scenario. In comparison, although the emissions of SO_2 and CO in the SSP 5–8.5 scenario also show a significant reduction from 2015 to 2050, other species, including NO_x and VOC, change within a much smaller magnitude compared to SSP 1-2.6 over China (Figure 3b). Furthermore, the emissions of O_3 precursors in eastern China remain at a high level in the future (Figures S9 and S10 in Supporting Information S1).

We applied the random forest algorithm (Section 3.2) with *S* derived from the GEOS-Chem simulation (described in Section 2.4), seasonal-mean Tmax and O_3 concentrations from CMIP6 models (Section 3.3.2) and the LAI in 2015 to examine future *P* values under SSP1-2.6 and SSP 5–8.5 scenarios. Future *S* value, seasonal-mean O_3 concentrations, and Tmax are shown in Figures S11–S13 in Supporting Information S1. The LAI values from MERRA2 were fixed in 2015 since the carbon cycles in most of the CMIP6 models remained large uncertainties (Arora et al., 2020). Figure 4 shows that the nationally averaged *P* values decreased to 29.9% in the 2050s following the SSP 1-2.6 scenario. The risk of the co-occurrences of O_3-polluted days and hot days was at a low level in most regions over China although the *P* values in North China remained at 48.7% in the 2050s. However, the *P* values under the SSP 5-8.5 scenario were predicted to remain high during the 2030–2050s with values ranging from 37.3% to 37.7% nationwide and 70.1%–70.5% averaged over North China. North Xinjiang Province, central eastern China, and northeast China all presented a high composited risk of O_3 exceedance during hot days.

Figure S13 in Supporting Information S1 shows the future number of hot days averaged from the 5 selected CMIP models under different scenarios. Following both SSP 1-2.6 and SSP 5–8.5 scenarios, the frequencies of hot days were highest in Northwest China from May to October. Since the strict reductions in anthropogenic carbon emissions (SSP 1-2.6) still failed to stop climate warming (Figure S14 in Supporting Information S1), the frequencies of hot days showed a slightly increasing trend over central eastern China from the 2030–2050s. SSP 5-8.5 witnessed a more rapid increase in the frequency of hot days compared to SSP 1-2.6. In particular, the number of hot days in North China increased from 12.1 days in the 2030s to 15.3 days in the 2050s, implying a higher risk of the co-occurrence of O_3-polluted days and hot days.

By multiplying the *P* values in Figure 4 and the number of hot days in Figure S13 in Supporting Information S1, we were able to predict the future frequencies of the co-occurrences of O_3-polluted days and hot days (Figure 5). Under the SSP 1-2.6 scenario, the composited risk of O_3 pollution during hot days significantly decreased, especially in North China, where the co-occurrence of O_3-polluted days and hot days decreased from 7.6 days

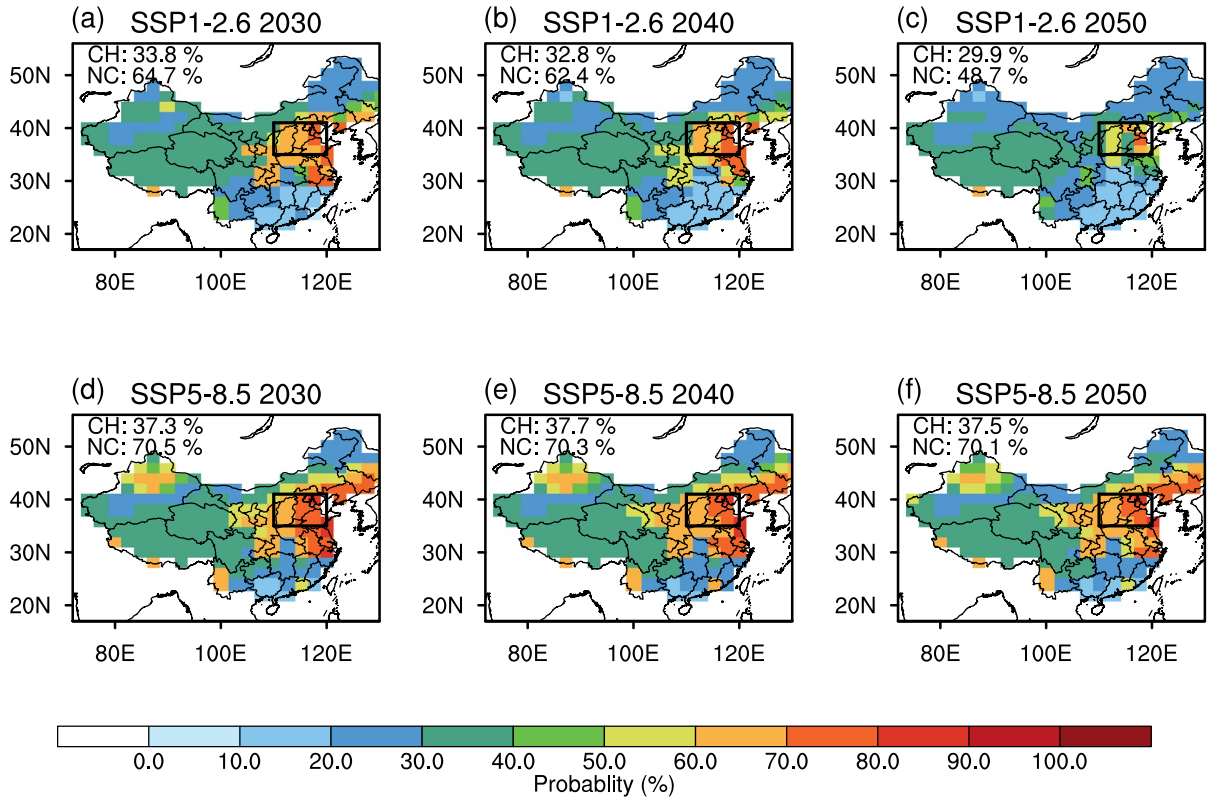

Figure 4. Spatial patterns of future *P* values predicted by the random forest algorithm under the Shared Socioeconomic Pathway (SSP) 1-2.6 and SSP 5-8.5 scenarios in the 2030, 2040, and 2050s. Numbers labeled "CH" and "NC" represent values averaged over China and North China, respectively.

in the 2030s to 4.9 days in the 2050s. However, SSP 5-8.5 predicted a worse future in which the co-occurrences of O_3-polluted days and hot days increased in North China from the 2030–2050s. These results implied large benefits in alleviating the composite risk of extreme weather events and severe air-polluted days through anthropogenic emission reductions.

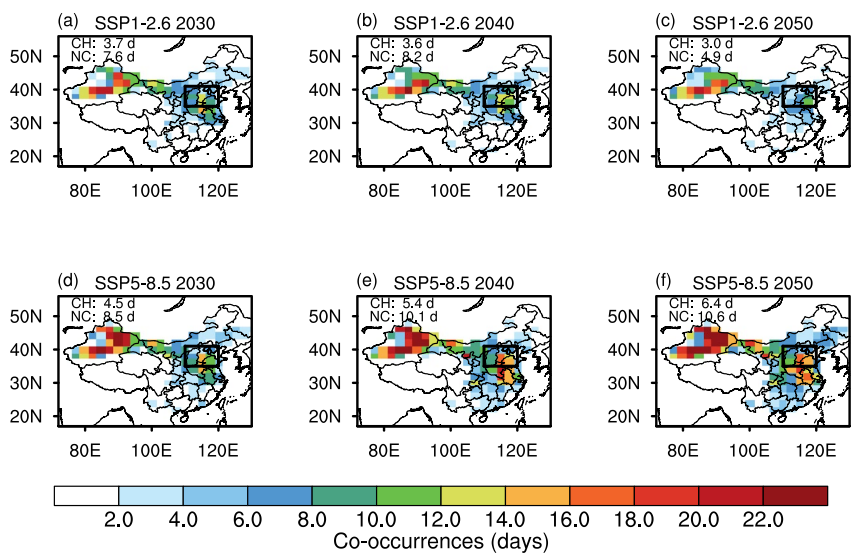

Figure 5. Spatial patterns of co-occurrences of O_3-polluted days and hot days under the Shared Socioeconomic Pathway (SSP) 1-2.6 and SSP 5-8.5 scenarios in the 2030, 2040, and 2050s. Numbers labeled "CH" and "NC" represent days averaged over China and North China, respectively.

3.5. Comparison Between the Chemistry Climate Model Predictions and the Random Forest Algorithm

We compared our predicted future co-occurrences of hot days and O_3-polluted days with the chemistry-climate model results from the UKESM1-0-LL, which to our knowledge was the only one model in CMIP6 that provide future daily temperature and hourly O_3 concentration data under both SSP 1-2.6 and SSP 5–8.5 scenarios. Note that the UKESM1-0-LL results here were with the "r1i1p1f2" variant so they were not included in our random forest algorithm (see the CMIP6 model description in Section 2.5).

To begin with, we evaluated the UKESM1-0-LL model performance by comparing the observed and simulated seasonal-mean Tmax and MDA8 O_3 concentrations over May–October in 2015 (Figure S15 in Supporting Information S1). The site-level observations and the origin model outputs with a resolution of 1.25° latitude × 1.875° longitude were both interpolated into 2° latitude × 2.5° longitude. Although the UKESM1-0-LL model-simulated reasonable patterns of seasonal-mean Tmax, the O_3 concentrations were strongly overestimated (normalized mean bias exceeding 50% over China), which would definitely bring in large uncertainties in future prediction. As a result, we revised the future simulated daily Tmax and MDA8 O_3 concentrations by applying the linear regression relationships (Figures S15d and S15h in Supporting Information S1) between observations and simulations in 2015 under different SSP scenarios, and then obtained the UKESM1-0-LL-predicted future co-occurrences of hot days and O_3-polluted days over China.

The UKESM1-0-LL predictions (after revision) in the 2050s showed high risks of co-occurrences of hot days and O_3-polluted days not only in North China but also in northwest China (Figure S16 in Supporting Information S1), especially under the SSP 5–8.5 scenario, which was similar to our results from the random forest algorithm (Figure 5). Furthermore, the UKESM1-0-LL model-predicted national averaged days of co-occurrences decreased from 3.8 days in 2030s to 1.9 days 2050s under the SSP 1-2.6 scenario, but increased from 6.9 days in the 2030s to 13.7 days in the 2050s under the SSP 5-8.5 scenario. Although the specific numbers were different from our predictions (Figure 5), which might led by the underestimates of P values in the random forest algorithm, especially in North China or the overestimates in O_3 concentrations in UKESM1-0-LL, the UKESM1-0-LL model generally predicted similar future spatiotemporal variations of co-occurrences of hot days and O_3-polluted days as our results, suggesting that our random forest algorithm was capable to achieve the prediction within the reasonable bias.

4. Conclusions and Discussions

In summary, we predicted the future climate penalty on O_3 pollution from the perspective of extreme cases, which, to our knowledge, has rarely been examined. Since multimodel simulations of future daily O_3 concentrations were unavailable, we aimed to derive the climatological risk factor P, which was the probability of O_3 exceedance during hot days, through a random forest algorithm and further predicted the future co-occurrence of O_3-polluted days and hot days. Evaluations showed that the random forest algorithm was capable to derive a reasonable pattern of P values with a mean bias lower than 10% in most regions over China despite the underestimates in North China. By combining GEOS-Chem simulations and CMIP6 multimodel outputs, our results showed that both the SSP 1-2.6 and SSP 5-8.5 scenarios increased the future hot days nationwide. The SSP 1–2.6 scenario significantly reduced the composite risks of O_3 exceedance during hot days with P values reduced from 64.7% in the 2030s to 48.7% in the 2050s due to the strict reductions in anthropogenic emissions. However, the P values remained high under the SSP 5-8.5 scenario in eastern China, thus leading to increases in the co-occurrences of O_3-polluted days and hot days until the 2050s.

Uncertainties in the predicted co-occurrences of O_3-polluted days and hot days may be caused by three factors: algorithm uncertainties, model data uncertainties, and exclusion of variations in terrestrial vegetation. First, the random forest algorithm showed insufficient ability to predict extremely high P values (Figure 2). Even though we have tried almost all related parameters as predictors in EX8 (Table 1), such underestimates remained. As a result, the predicted P values under the SSP 5-8.5 scenario shown in Figure 4 might be underestimated, further underestimating the future co-occurrence of O_3-polluted days and hot days. Second, although we applied the ensemble mean from the multimodel outputs to avoid the problem of model dependence, uncertainties could still be induced by large discrepancies in variables among different CMIP6 models, especially for the prediction of future hot days (Figure S17 in Supporting Information S1). Meanwhile, all 5 selected climate models overestimated the number of hot days in northwest China (Figure S7 in Supporting Information S1), which might

exaggerate the co-occurrence days in Xinjiang Province as shown in Figure 5. Furthermore, the variations in terrestrial vegetation could influence O_3 concentrations through BVOCs emissions and stomatal dry depositions on decadal time scales (Lin et al., 2020; Wang et al., 2020), which were not considered in this study because most of the CMIP6 models lacked a dynamic vegetation module (Arora et al., 2020); thus, large uncertainties remained in predicting future vegetation.

Our approach applied the O_3-Tmax sensitivity rather than the direct NO_x and VOCs emissions (Table 1) because it seems difficult for the random forest to well represent the complex nonlinear chemical reactions with only emission inputs (Keller & Evans, 2019). We tried to replace the *S* value with the NO_x and VOCs emissions in EX5 but found out random forest score of 0.64 and an RMSE value of 17.2% between observed and random-forest-predicted *P* values over China (not shown in Table 1), indicating a poorer performance compared to the origin EX5 configuration. Nevertheless, using the GEOS-Chem model to describe future *S* values still brought in new uncertainties considering the model bias (Figure S4 in Supporting Information S1) and fixed meteorological fields. A dilemma was confronted that either suffering the low performance of random forest with exact emissions or admitting the simulated bias in a global transport chemistry model. However, it should be clarified that despite the direct NO_x and VOCs emissions were omitted (Table 1), future changes in anthropogenic emissions under different SSP scenarios were comprehensively considered in our approach through the GEOS-Chem-simulated *S* values.

Despite the uncertainties, we established an effective machine learning method to predict the composite risks of the co-occurrences of extreme weather events and air-polluted days by considering future changes in both anthropogenic emissions and climate. The algorithm avoided the model dependence problem by taking full advantage of the CMIP6 multimodel outputs. Our results highlight that the reductions in anthropogenic emissions can significantly alleviate O_3 pollution during hot days with the implications of benefits of reducing the related health risks.

Data Availability Statement

Observed ozone (O_3) concentrations are obtained from the China Ministry of Ecology and Environment (http://www.cnemc.cn). Ground-level-observed meteorological parameters are obtained from ground-level weather monitoring stations maintained by the China Meteorological Administration (http://data.cma.cn/). The CMIP6 model outputs are downloaded from https://esgf-node.llnl.gov/projects/cmip6/. GEOS-Chem-simulated O_3 data can be assessed from https://zenodo.org/record/6504889#.YmvZZJPP2rM.

Acknowledgments
This work was supported by the National Natural Science Foundation of China (Grant No. 42021004) and the National Key Research and Development Program of China (Grant No. 2019YFA0606800).

References

Analitis, A., Michelozzi, P., D'Ippoliti, D., de'Donato, F., Menne, B., Matthies, F., et al. (2014). Effects of heat waves on mortality effect modification and confounding by air pollutants. *Epidemiology*, *25*(1), 15–22. https://doi.org/10.1097/ede.0b013e31828ac01b

Araki, S., Shima, M., & Yamamoto, K. (2018). Spatiotemporal land use random forest model for estimating metropolitan NO2 exposure in Japan. *The Science of the Total Environment*, *634*, 1269–1277. https://doi.org/10.1016/j.scitotenv.2018.03.324

Arora, V. K., Katavouta, A., Williams, R. G., Jones, C. D., Brovkin, V., Friedlingstein, P., et al. (2020). Carbon-concentration and carbon-climate feedbacks in CMIP6 models and their comparison to CMIP5 models. *Biogeosciences*, *17*(16), 4173–4222. https://doi.org/10.5194/bg-17-4173-2020

Bey, I., Jacob, D. J., Yantosca, R. M., Logan, J. A., Field, B. D., Fiore, A. M., et al. (2001). Global modeling of tropospheric chemistry with assimilated meteorology: Model description and evaluation. *Journal of Geophysical Research*, *106*(D19), 23073–23095. https://doi.org/10.1029/2001jd000807

Bloomer, B. J., Stehr, J. W., Piety, C. A., Salawitch, R. J., & Dickerson, R. R. (2009). Observed relationships of ozone air pollution with temperature and emissions. *Geophysical Research Letters*, *36*. https://doi.org/10.1029/2009gl037308

Breiman, L. (2001). Random forests. *Machine Learning*, *45*(1), 5–32. https://doi.org/10.1023/a:1010933404324

Chen, G., Li, S., Knibbs, L. D., Hamm, N. A. S., Cao, W., Li, T., et al. (2018). A machine learning method to estimate PM2.5 concentrations across China with remote sensing, meteorological and land use information. *The Science of the Total Environment*, *636*, 52–60. https://doi.org/10.1016/j.scitotenv.2018.04.251

Clifton, O. E., Fiore, A. M., Massman, W. J., Baublitz, C. B., Coyle, M., Emberson, L., et al. (2020). Dry deposition of ozone over land: Processes, measurement, and modeling. *Review of Geophysics*, *58*(1), e2019RG000670. https://doi.org/10.1029/2019RG000670

Colette, A., Andersson, C., Baklanov, A., Bessagnet, B., Brandt, J., Christensen, J. H., et al. (2015). Is the ozone climate penalty robust in Europe? *Environmental Research Letters*, *10*(8), 084015. https://doi.org/10.1088/1748-9326/10/8/084015

Dang, R., & Liao, H. (2019). Severe winter haze days in the Beijing-Tianjin-Hebei region from 1985 to 2017 and the roles of anthropogenic emissions and meteorology. *Atmospheric Chemistry and Physics*, *19*(16), 10801–10816. https://doi.org/10.5194/acp-19-10801-2019

Dawson, J. P., Adams, P. J., & Pandis, S. N. (2007). Sensitivity of ozone to summertime climate in the eastern USA: A modeling case study. *Atmospheric Environment*, *41*(7), 1494–1511. https://doi.org/10.1016/j.atmosenv.2006.10.033

Ding, T., Qian, W., & Yan, Z. (2010). Changes in hot days and heat waves in China during 1961–2007. *International Journal of Climatology*, *30*(10), 1452–1462. https://doi.org/10.1002/joc.1989

Fleming, Z. L., Doherty, R. M., Von Schneidemesser, E., Malley, C. S., Cooper, O. R., Pinto, J. P., et al. (2018). *Tropospheric Ozone Assessment Report: Present-Day Ozone Distribution and Trends Relevant to Human Health* (Vol. 6). Elementa-Science of the Anthropocene. https://doi.org/10.1525/elementa.273

Fu, T.-M., & Tian, H. (2019). Climate change penalty to ozone air quality: Review of current understandings and knowledge gaps. *Current Pollution Reports*, *5*(3), 159–171. https://doi.org/10.1007/s40726-019-00115-6

Fu, T.-M., Zheng, Y., Paulot, F., Mao, J., & Yantosca, R. M. (2015). Positive but variable sensitivity of August surface ozone to large-scale warming in the southeast United States. *Nature Climate Change*, *5*(5), 454–458. https://doi.org/10.1038/nclimate2567

Gong, C., & Liao, H. (2019). A typical weather pattern for ozone pollution events in North China. *Atmospheric Chemistry and Physics*, *19*(22), 13725–13740. https://doi.org/10.5194/acp-19-13725-2019

Gong, C., Liao, H., Yue, X., Ma, Y., & Lei, Y. (2021). Impacts of ozone-vegetation interactions on ozone pollution episodes in North China and the Yangtze river delta. *Geophysical Research Letters*, *48*(12), e2021GL093814. https://doi.org/10.1029/2021gl093814

Gong, C., Liao, H., Zhang, L., Yue, X., Dang, R., & Yang, Y. (2020). Persistent ozone pollution episodes in North China exacerbated by regional transport. *Environmental pollution*, *265*, 115056. https://doi.org/10.1016/j.envpol.2020.115056

Gong, C., Yue, X., Liao, H., & Ma, Y. (2021). A humidity-based exposure index representing ozone damage effects on vegetation. *Environmental Research Letters*, *16*(4). https://doi.org/10.1088/1748-9326/abecbb

Gu, Y., Li, K., Xu, J., Liao, H., & Zhou, G. (2020). *Observed dependence of surface ozone on increasing temperature in Shanghai*. Atmospheric Environment, 221. https://doi.org/10.1016/j.atmosenv.2019.117108

Guenther, A. B., Jiang, X., Heald, C. L., Sakulyanontvittaya, T., Duhl, T., Emmons, L. K., & Wang, X. (2012). The model of emissions of Gases and aerosols from nature version 2.1 (MEGAN2.1): An extended and updated framework for modeling biogenic emissions. *Geoscientific Model Development*, *5*(6), 1471–1492. https://doi.org/10.5194/gmd-5-1471-2012

He, H., Hembeck, L., Hosley, K. M., Canty, T. P., Salawitch, R. J., & Dickerson, R. R. (2013). High ozone concentrations on hot days: The role of electric power demand and NO_x emissions. *Geophysical Research Letters*, *40*(19), 5291–5294. https://doi.org/10.1002/grl.50967

Jacob, D. J., & Winner, D. A. (2009). Effect of climate change on air quality. *Atmospheric Environment*, *43*(1), 51–63. https://doi.org/10.1016/j.atmosenv.2008.09.051

Jing, P., Lu, Z., & Steiner, A. L. (2017). The ozone-climate penalty in the Midwestern US. *Atmospheric Environment*, *170*, 130–142. https://doi.org/10.1016/j.atmosenv.2017.09.038

Kaminska, J. A. (2019). A random forest partition model for predicting NO2 concentrations from traffic flow and meteorological conditions. *The Science of the Total Environment*, *651*, 475–483. https://doi.org/10.1016/j.scitotenv.2018.09.196

Keller, C. A., & Evans, M. J. (2019). Application of random forest regression to the calculation of gas-phase chemistry within the GEOS-Chem chemistry model v10. *Geoscientific Model Development*, *12*(3), 1209–1225. https://doi.org/10.5194/gmd-12-1209-2019

Kleinman, L. I., Daum, P. H., Lee, Y. N., Nunnermacker, L. J., Springston, S. R., Weinstein-Lloyd, J., & Rudolph, J. (2002). Ozone production efficiency in an urban area. *Journal of Geophysical Research*, *107*(D23). https://doi.org/10.1029/2002jd002529

Kuerban, M., Waili, Y., Fan, F., Liu, Y., Qin, W., Dore, A. J., et al. (2020). Spatio-temporal patterns of air pollution in China from 2015 to 2018 and implications for health risks. *Environmental Pollution*, *258*. https://doi.org/10.1016/j.envpol.2019.113659

Lamarque, J. F., Shindell, D. T., Josse, B., Young, P. J., Cionni, I., Eyring, V., et al. (2013). The atmospheric chemistry and climate model Intercomparison Project (ACCMIP): Overview and description of models, simulations and climate diagnostics. *Geoscientific Model Development*, *6*(1), 179–206. https://doi.org/10.5194/gmd-6-179-2013

Lelieveld, J., Evans, J. S., Fnais, M., Giannadaki, D., & Pozzer, A. (2015). The contribution of outdoor air pollution sources to premature mortality on a global scale. *Nature*, *525*(7569), 367–371. https://doi.org/10.1038/nature15371

Li, K., Jacob, D. J., Liao, H., Qiu, Y., Shen, L., Zhai, S., et al. (2021). Ozone pollution in the North China Plain spreading into the late-winter haze season. *Proceedings of the National Academy of Sciences*, *118*(10). https://doi.org/10.1073/pnas.2015797118

Li, K., Jacob, D. J., Liao, H., Shen, L., Zhang, Q., & Bates, K. H. (2019). Anthropogenic drivers of 2013–2017 trends in summer surface ozone in China. *Proceedings of the National Academy of Sciences*, *116*(2), 422–427. https://doi.org/10.1073/pnas.1812168116

Lin, J.-T., & McElroy, M. B. (2010). Impacts of boundary layer mixing on pollutant vertical profiles in the lower troposphere: Implications to satellite remote sensing. *Atmospheric Environment*, *44*(14), 1726–1739. https://doi.org/10.1016/j.atmosenv.2010.02.009

Lin, M., Horowitz, L. W., Xie, Y., Paulot, F., Malyshev, S., Shevliakova, E., et al. (2020). Vegetation feedbacks during drought exacerbate ozone air pollution extremes in Europe. *Nature Climate Change*, *10*(5), 444–451. https://doi.org/10.1038/s41558-020-0743-y

Lombardozzi, D., Levis, S., Bonan, G., Hess, P. G., & Sparks, J. P. (2015). The influence of chronic ozone exposure on global carbon and water cycles. *Journal of Climate*, *28*(1), 292–305. https://doi.org/10.1175/jcli-d-14-00223.1

Lu, X., Hong, J., Zhang, L., Cooper, O. R., Schultz, M. G., Xu, X., et al. (2018). Severe surface ozone pollution in China: A global perspective. *Environmental Science and Technology Letters*, *5*(8), 487–494. https://doi.org/10.1021/acs.estlett.8b00366

Lu, X., Zhang, L., Chen, Y., Zhou, M., Zheng, B., Li, K., et al. (2019). Exploring 2016–2017 surface ozone pollution over China: Source contributions and meteorological influences. *Atmospheric Chemistry and Physics*, *19*(12), 8339–8361. https://doi.org/10.5194/acp-19-8339-2019

Lu, X., Zhang, L., Wang, X., Gao, M., Li, K., Zhang, Y., et al. (2020). Rapid increases in warm-season surface ozone and resulting health impact in China since 2013. *Environmental Science and Technology Letters*, *7*(4), 240–247. https://doi.org/10.1021/acs.estlett.0c00171

Ma, M., Gao, Y., Wang, Y., Zhang, S., Leung, L. R., Liu, C., et al. (2019). Substantial ozone enhancement over the North China Plain from increased biogenic emissions due to heat waves and land cover in summer 2017. *Atmospheric Chemistry and Physics*, *19*(19), 12195–12207. https://doi.org/10.5194/acp-19-12195-2019

McLinden, C. A., Olsen, S. C., Hannegan, B., Wild, O., Prather, M. J., & Sundet, J. (2000). Stratospheric ozone in 3-D models: A simple chemistry and the cross-tropopause flux. *Journal of Geophysical Research*, *105*(D11), 14653–14665. https://doi.org/10.1029/2000jd900124

Meehl, G. A., Tebaldi, C., Tilmes, S., Lamarque, J.-F., Bates, S., Pendergrass, A., & Lombardozzi, D. (2018). Future heat waves and surface ozone. *Environmental Research Letters*, *13*(6). https://doi.org/10.1088/1748-9326/aabcdc

Meinshausen, M., Nicholls, Z. R. J., Lewis, J., Gidden, M. J., Vogel, E., Freund, M., et al. (2020). The shared socio-economic pathway (SSP) greenhouse gas concentrations and their extensions to 2500. *Geoscientific Model Development*, *13*(8), 3571–3605. https://doi.org/10.5194/gmd-13-3571-2020

Park, R. J., Jacob, D. J., Chin, M., & Martin, R. V. (2003). Sources of carbonaceous aerosols over the United States and implications for natural visibility. *Journal of Geophysical Research*, *108*(D12). https://doi.org/10.1029/2002jd003190

Pedregosa, F., Varoquaux, G., Gramfort, A., Michel, V., Thirion, B., Grisel, O., et al. (2011). Scikit-learn: Machine learning in Python. *Journal of Machine Learning Research*, *12*, 2825–2830.

Perkins-Kirkpatrick, S. E., & Lewis, S. C. (2020). Increasing trends in regional heatwaves. *Nature Communications*, *11*(1). https://doi.org/10.1038/s41467-020-16970-7

Porter, W. C., & Heald, C. L. (2019). The mechanisms and meteorological drivers of the summertime ozone–temperature relationship. *Atmospheric Chemistry and Physics*, *19*(21), 13367–13381. https://doi.org/10.5194/acp-19-13367-2019

Pu, X., Wang, T. J., Huang, X., Melas, D., Zanis, P., Papanastasiou, D. K., & Poupkou, A. (2017). Enhanced surface ozone during the heat wave of 2013 in Yangtze River Delta region, China. *The Science of the Total Environment*, *603–604*, 807–816. https://doi.org/10.1016/j.scitotenv.2017.03.056

Pye, H. O. T., Liao, H., Wu, S., Mickley, L. J., Jacob, D. J., Henze, D. K., & Seinfeld, J. H. (2009). Effect of changes in climate and emissions on future sulfate-nitrate-ammonium aerosol levels in the United States. *Journal of Geophysical Research*, *114*. https://doi.org/10.1029/2008jd010701

Rasmussen, D. J., Hu, J., Mahmud, A., & Kleeman, M. J. (2013). The ozone-climate penalty: Past, present, and future. *Environmental Science & Technology*, *47*(24), 14258–14266. https://doi.org/10.1021/es403446m

Schnell, J. L., & Prather, M. J. (2017). Co-occurrence of extremes in surface ozone, particulate matter, and temperature over eastern North America. *Proceedings of the National Academy of Sciences of the U S A*, *114*(11), 2854–2859. https://doi.org/10.1073/pnas.1614453114

Schnell, J. L., Prather, M. J., Josse, B., Naik, V., Horowitz, L. W., Zeng, G., et al. (2016). Effect of climate change on surface ozone over North America, Europe, and East Asia. *Geophysical Research Letters*, *43*(7), 3509–3518. https://doi.org/10.1002/2016gl068060

Shi, Z., Huang, L., Li, J., Ying, Q., Zhang, H., & Hu, J. (2020). Sensitivity analysis of the surface ozone and fine particulate matter to meteorological parameters in China. *Atmospheric Chemistry and Physics*, *20*(21), 13455–13466. https://doi.org/10.5194/acp-20-13455-2020

Sillman, S. (1999). The relation between ozone, NOx and hydrocarbons in urban and polluted rural environments. *Atmospheric Environment*, *33*(12), 1821–1845. https://doi.org/10.1016/s1352-2310(98)00345-8

Solberg, S., Hov, O., Sovde, A., Isaksen, I. S. A., Coddeville, P., De Backer, H., et al. (2008). European surface ozone in the extreme summer 2003. *Journal of Geophysical Research: Atmospheres*, *113*(D7). https://doi.org/10.1029/2007jd009098

Steiner, A. L., Tonse, S., Cohen, R. C., Goldstein, A. H., & Harley, R. A. (2006). Influence of future climate and emissions on regional air quality in California. *Journal of Geophysical Research: Atmospheres*, *111*(D18). https://doi.org/10.1029/2005jd006935

Wang, L., Tai, A. P. K., Tam, C.-Y., Sadiq, M., Wang, P., & Cheung, K. K. W. (2020). Impacts of future land use and land cover change on mid-21st-century surface ozone air quality: Distinguishing between the biogeophysical and biogeochemical effects. *Atmospheric Chemistry and Physics*, *20*(19), 11349–11369. https://doi.org/10.5194/acp-20-11349-2020

Wang, W. N., Cheng, T.-H., Gu, X.-F., Chen, H., Guo, H., Wang, Y., et al. (2017). Assessing spatial and temporal patterns of observed ground-level ozone in China. *Scientific Reports*, *7*(1), 3651. https://doi.org/10.1038/s41598-017-03929-w

Wang, Y., Du, Y., Wang, J., & Li, T. (2019). *Calibration of a Low-Cost PM2.5 Monitor Using a Random Forest Model* (Vol. 133). Environment International. https://doi.org/10.1016/j.envint.2019.105161

Wang, Y., Zhang, Y., Hao, J., & Luo, M. (2011). Seasonal and spatial variability of surface ozone over China: Contributions from background and domestic pollution. *Atmospheric Chemistry and Physics*, *11*(7), 3511–3525. https://doi.org/10.5194/acp-11-3511-2011

Wei, J., Huang, W., Li, Z., Xue, W., Peng, Y., Sun, L., & Cribb, M. (2019). *Estimating 1-km-resolution PM2.5 concentrations across China using the space-time random forest approach*. Remote Sensing of Environment, 231. https://doi.org/10.1016/j.rse.2019.111221

Wei, W., Fang, Y., & Zhou, Y. (2021). Synoptic and meteorological drivers of regional ozone pollution events in China. *Environmental Research Communications*, *3*(5). https://doi.org/10.1088/2515-7620/abfe9c

Wu, S., Mickley, L. J., Leibensperger, E. M., Jacob, D. J., Rind, D., & Streets, D. G. (2008). Effects of 2000–2050 global change on ozone air quality in the United States. *Journal of Geophysical Research*, *113*(D6). https://doi.org/10.1029/2007jd008917

Yue, X., Unger, N., Harper, K., Xia, X., Liao, H., Zhu, T., et al. (2017). Ozone and haze pollution weakens net primary productivity in China. *Atmospheric Chemistry and Physics*, *17*(9), 6073–6089. https://doi.org/10.5194/acp-17-6073-2017

Zhan, Y., Luo, Y., Deng, X., Grieneisen, M. L., Zhang, M., & Di, B. (2018). Spatiotemporal prediction of daily ambient ozone levels across China using random forest for human exposure assessment. *Environmental Pollution*, *233*, 464–473. https://doi.org/10.1016/j.envpol.2017.10.029

Zhao, S., Pappin, A. J., Mesbah, S. M., Zhang, J. Y. J., MacDonald, N. L., & Hakami, A. (2013). Adjoint estimation of ozone climate penalties. *Geophysical Research Letters*, *40*(20), 5559–5563. https://doi.org/10.1002/2013gl057623

Zheng, B., Tong, D., Li, M., Liu, F., Hong, C., Geng, G., et al. (2018). Trends in China's anthropogenic emissions since 2010 as the consequence of clean air actions. *Atmospheric Chemistry and Physics*, *18*(19), 14095–14111. https://doi.org/10.5194/acp-18-14095-2018